Physics Letters A 384 (2020) 126234

Contents lists available at ScienceDirect

Physics Letters A

www.elsevier.com/locate/pla

Controlling self-Kerr nonlinearity with an external magnetic field in a degenerate two-level inhomogeneously broadened medium

Nguyen Huy Bang, Dinh Xuan Khoa, Le Van Doai *

Vinh University, 182 Le Duan Street, Vinh City, Viet Nam

ARTICLE INFO

Article history:
Received 6 November 2019
Received in revised form 25 December 2019
Accepted 28 December 2019
Available online 8 January 2020
Communicated by V.A. Markel

Keywords:
Electromagnetically induced transparency
Kerr nonlinearity
Magnetic field

ABSTRACT

The magnitude and sign of self-Kerr nonlinear coefficient in a degenerate two-level inhomogeneously broadened medium are simply controlled by an external magnetic field. By changing the external magnetic field we can switch a negative peak of Kerr nonlinear coefficient into a positive peak and vice versa, and transform a zero value of Kerr nonlinear coefficient into a positive or negative peak in resonant region. Such a controllable Kerr nonlinear coefficient can be used to manipulate the working characteristics of photonic devices such as optical switches and bistable elements.

© 2020 Elsevier B.V. All rights reserved.

1. Introduction

It is known that self-Kerr nonlinear coefficient plays an important role in optical nonlinear effects such as optical switching and bistability, generation of optical solitons, multi-wave mixing converters, and so on. In such applications, controllable and large nonlinear coefficient is often needed to gain conversion efficiency and optimize optical nonlinear processes. Over the past decades, the advent of electromagnetically induced transparency (EIT) [1] has opened up an excellent route to obtain giant nonlinearity with vanishing absorption [2]. Therefore, the EIT medium becomes ideal to achieve nonlinear optical effects at very low light intensities [3].

Using the EIT technique, Wang et al., [4] first measured self-Kerr nonlinear coefficient in a three-level lambda atomic system under Doppler broadening by using the ring cavity. It is shown that the Kerr nonlinear coefficient can be enhanced in several orders of the magnitude owing to the presence of EIT. Simultaneously, the amplitude and the sign of nonlinearity can be controlled simply by tuning the frequency or the intensity of coupling field. Since then, many proposals have been suggested for the enhancement and the control of nonlinear coefficient via spontaneously generated coherence (SGC) and the relative phase of applied laser fields [5–9], the microwave field [10], and the electric field [11]. Recent studies on the Kerr nonlinearity have been done in four-level [12–14] and five-level systems [7,15–18] in which the nonlinearity can be enhanced and controlled at multiple frequencies.

In recent years, the studies have also been focused on the utilization of external magnetic field to control optical properties of the atomic medium. For example, the effect of the magnetic field on the EIT [19–27], slow or fast light propagation [28,29], optical switching and bistability [30–33] have investigated. However, controlling the nonlinear coefficient by an external magnetic field has not been explored so far. In this paper, we suggest using an external magnetic field as a "knob" to control the magnitude and the sign of self-Kerr nonlinear coefficient in a degenerate two-level inhomogeneously broadened medium. An analytical expression for self-Kerr nonlinear coefficient is derived under Doppler broadening. The influences of the external magnetic field, the intensity and frequency of coupling field as well as the temperature on the magnitude and the sign of the Kerr coefficient are studied.

2. Theoretical model

The degenerate two-level atomic system interacting with the two laser fields is shown in Fig. 1(a). A weak probe field E_p with the left-circularly polarized component σ^- (having angular frequency ω_p) applies to the transition $|1\rangle \leftrightarrow |2\rangle$, while the transition $|2\rangle \leftrightarrow |3\rangle$ is driven by a strong coupling field E_c with the right-circularly polarized component σ^+ (having angular frequency ω_c). In order to eliminate first-order Doppler effect, we choose the coupling beam which is co-propagating with the probe beam. The degenerate two-level atomic system is placed in an external magnetic field (B) parallel to the propagation direction of the probe and coupling fields. This is used to remove the degeneracy among the ground-state sublevels $|1\rangle$ and $|3\rangle$ via the Zeeman effect and to form the three-level lambda system as shown in Fig. 1(b). The Zee-

* Corresponding author.
E-mail address: doaivatly@gmail.com (L.V. Doai).

https://doi.org/10.1016/j.physleta.2020.126234
0375-9601/© 2020 Elsevier B.V. All rights reserved.

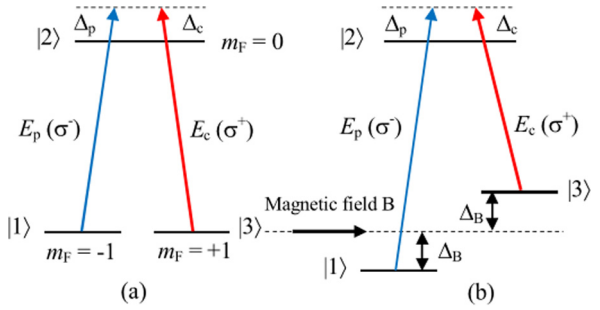

Fig. 1. (a) Degenerate two-level atomic system, (b) three-level lambda system is formed in the presence of an external magnetic field, where the state $|1\rangle$ is lowered while the state $|3\rangle$ is lifted by the same amount Δ_B corresponding to the Zeeman shift.

man shift of levels $|1\rangle$ and $|3\rangle$ is given by [31] $\hbar\Delta_B = \mu_B m_F g_F B$ where μ_B is the Bohr magneton, g_F is the Landé factor, and $m_F = \pm 1$ is the magnetic quantum number of the corresponding state. We denote γ_{21} and γ_{23} are respectively the decay rates from the state $|2\rangle$ to the states $|1\rangle$ and $|3\rangle$, while γ_{31} is the relaxation rate of atomic coherence between the ground states $|1\rangle$ and $|3\rangle$ by collisions of hot atoms.

Under electric-dipole and rotating-wave approximations, the evolution of the system is described by the following density-matrix equations:

$$\dot{\rho}_{11} = \gamma_{31}(\rho_{33} - \rho_{11}) + \gamma_{21}\rho_{22} - \frac{i}{2}\Omega_p\rho_{21} + \frac{i}{2}\Omega_p\rho_{12}, \tag{1a}$$

$$\dot{\rho}_{33} = \gamma_{31}(\rho_{11} - \rho_{33}) + \gamma_{23}\rho_{22} + \frac{i}{2}\Omega_c\rho_{32} - \frac{i}{2}\Omega_c\rho_{23}, \tag{1b}$$

$$\dot{\rho}_{22} = -(\gamma_{23} + \gamma_{21})\rho_{22} - \frac{i}{2}\Omega_p\rho_{12} + \frac{i}{2}\Omega_p\rho_{21} - \frac{i}{2}\Omega_c\rho_{32} + \frac{i}{2}\Omega_c\rho_{23}, \tag{1c}$$

$$\dot{\rho}_{21} = -[\gamma - i(\Delta_p - \Delta_B)]\rho_{21} + \frac{i}{2}\Omega_p(\rho_{22} - \rho_{11}) - \frac{i}{2}\Omega_c\rho_{31}, \tag{1d}$$

$$\dot{\rho}_{23} = -[\gamma - i(\Delta_c + \Delta_B)]\rho_{23} + \frac{i}{2}\Omega_c(\rho_{22} - \rho_{33}) - \frac{i}{2}\Omega_p\rho_{13}, \tag{1e}$$

$$\dot{\rho}_{31} = -[\gamma_{31} - i(\Delta_p - \Delta_c - 2\Delta_B)]\rho_{31} + \frac{i}{2}\Omega_p\rho_{32} - \frac{i}{2}\Omega_c\rho_{21}, \tag{1f}$$

$$\rho_{nm} = \rho^*_{mn}, \tag{1g}$$

$$\rho_{11} + \rho_{22} + \rho_{33} = 1, \tag{1h}$$

where $\gamma = \frac{\gamma_{21}+\gamma_{23}+\gamma_{31}}{2}$. $\Delta_p = \omega_p - \omega_{21}$ and $\Delta_c = \omega_c - \omega_{23}$ are the frequency detuning of the probe and coupling beam, respectively. $\Omega_p = \frac{d_{21}E_p}{\hbar}$ and $\Omega_c = \frac{d_{23}E_c}{\hbar}$ are respectively the Rabi frequency of the probe and coupling fields with d_{mn} being the electric-dipole matrix element associated with the transition from the state $|m\rangle$ to the state $|n\rangle$.

In order to compute the linear and nonlinear susceptibilities, we solve the density matrix equations (1) perturbatively to third order under the steady state condition $\partial\rho/\partial t = 0$. That is, the density matrix elements are described by

$$\rho_{mn} = \rho^{(0)}_{mn} + \rho^{(1)}_{mn} + \cdots \rho^{(n)}_{mn}, \tag{2}$$

where each successive approximation is calculated by using the density-matrix elements of one order less than the one being calculated. We assume that initially the population is in the ground states $|1\rangle$ and $|3\rangle$ with the same populations, namely, $\rho^{(0)}_{11} \approx \rho^{(0)}_{33} \approx 1/2$, and $\rho^{(0)}_{22} \approx 0$.

From Eqs. (1d) and (1f), and by using the weak-probe approximation we found the solution to ρ_{21} in first-order as

$$\rho^{(1)}_{21} = \frac{\frac{i}{2}\Omega_p(\rho^{(0)}_{22} - \rho^{(0)}_{11})}{\gamma - i(\Delta_p - \Delta_B) + \frac{(\Omega_c/2)^2}{\gamma_{31} - i(\Delta_p - \Delta_c - 2\Delta_B)}} \approx \frac{-i\Omega_p}{4Z}, \tag{3}$$

with

$$Z = \gamma - i(\Delta_p - \Delta_B) + \frac{(\Omega_c/2)^2}{\gamma_{31} - i(\Delta_p - \Delta_c - 2\Delta_B)}. \tag{4}$$

In the same way, we can obtain the expression for ρ_{21} in third-order as

$$\rho^{(3)}_{21} = \frac{\frac{i}{2}\Omega_p(\rho^{(2)}_{22} - \rho^{(2)}_{11})}{Z}. \tag{5}$$

Thus, in order to calculate third order in ρ_{21} we need to determine $\rho_{22} - \rho_{11}$ to second order. We assume that $\rho^{(2)}_{33} \approx 0$, and notice that $\rho^{(2)}_{11} + \rho^{(2)}_{22} + \rho^{(2)}_{33} = 0$. Therefore, from Eqs. (1a) and (1c), the expression for $\rho^{(2)}_{22} - \rho^{(2)}_{11}$ can be derived as

$$\rho^{(2)}_{22} - \rho^{(2)}_{11} = \frac{2}{2\gamma + \gamma_{21}}[i\Omega_p\rho^{(1)}_{21} - i\Omega_p\rho^{(1)}_{12}] + \frac{2\gamma_{31}}{2\gamma + \gamma_{21}}, \tag{6a}$$

$$= \frac{\Omega_p^2}{2(2\gamma + \gamma_{21})}\left(\frac{1}{Z} + \frac{1}{Z*}\right) + \frac{2\gamma_{31}}{2\gamma + \gamma_{21}}. \tag{6b}$$

With the above procedure, ρ_{21} is calculated in third order as:

$$\rho^{(3)}_{21} = \frac{\Omega_p^2}{2\gamma + \gamma_{21}}\frac{i\Omega_p}{4Z}\left[\frac{1}{Z} + \frac{1}{Z^*}\right] + \frac{i\Omega_p}{Z}\frac{\gamma_{31}}{2\gamma + \gamma_{21}}. \tag{7}$$

Having $\rho^{(1)}_{21}$ and $\rho^{(3)}_{21}$, the matrix element ρ_{21} is determined up to third-order as

$$\rho_{21} = \rho^{(1)}_{21} + \rho^{(3)}_{21} = \frac{-i\Omega_p}{4Z}\left(1 - \frac{4\gamma_{31}}{2\gamma + \gamma_{21}}\right) + \frac{i\Omega_p}{4Z}\frac{\Omega_p^2}{2\gamma + \gamma_{21}}\left(\frac{1}{Z} + \frac{1}{Z^*}\right), \tag{8}$$

where Z^* is the complex conjugation of Z.

The total susceptibility χ for the probe light is represented by

$$\chi = -2\frac{Nd_{21}}{\varepsilon_0 E_p}\rho_{21} = \frac{Nd_{21}}{\varepsilon_0 E_p}\left[\frac{i\Omega_p}{2Z}\left(1 - \frac{4\gamma_{31}}{2\gamma + \gamma_{21}}\right) - \frac{i\Omega_p}{4Z}\frac{\Omega_p^2}{2\gamma + \gamma_{21}}\left(\frac{1}{Z} + \frac{1}{Z^*}\right)\right]. \tag{9}$$

On the other hand, the total susceptibility can be written in an alternative form as

$$\chi = \chi^{(1)} + 3E_p^2\chi^{(3)}. \tag{10}$$

By comparing Eqs. (9) and (10), the first-order susceptibility $\chi^{(1)}$ and the third-order susceptibility $\chi^{(3)}$ can be derived as

$$\chi^{(1)} = \frac{iNd_{21}^2}{\varepsilon_0\hbar}\frac{1}{2Z}\left(1 - \frac{4\gamma_{31}}{2\gamma + \gamma_{21}}\right), \tag{11}$$

$$\chi^{(3)} = -\frac{iNd_{21}^4}{6\varepsilon_0\hbar^3}\frac{1}{2\gamma + \gamma_{21}}\frac{1}{Z}\left(\frac{1}{Z} + \frac{1}{Z^*}\right). \tag{12}$$

For hot atoms, the Doppler effect is needed to be included. In this configuration, the coupling and probe beams co-propagate through the atomic medium. Therefore, an atom with velocity v moving towards probe beam will see an up-shift frequency of the probe and coupling lasers as $\omega_p + (v/c)\omega_p$ and $\omega_c + (v/c)\omega_c$, respectively. In such cases, the frequency detuning of the laser beams is adjusted accordingly as $\Delta'_p = \Delta_p + (v/c)\omega_p$ and $\Delta'_c =$

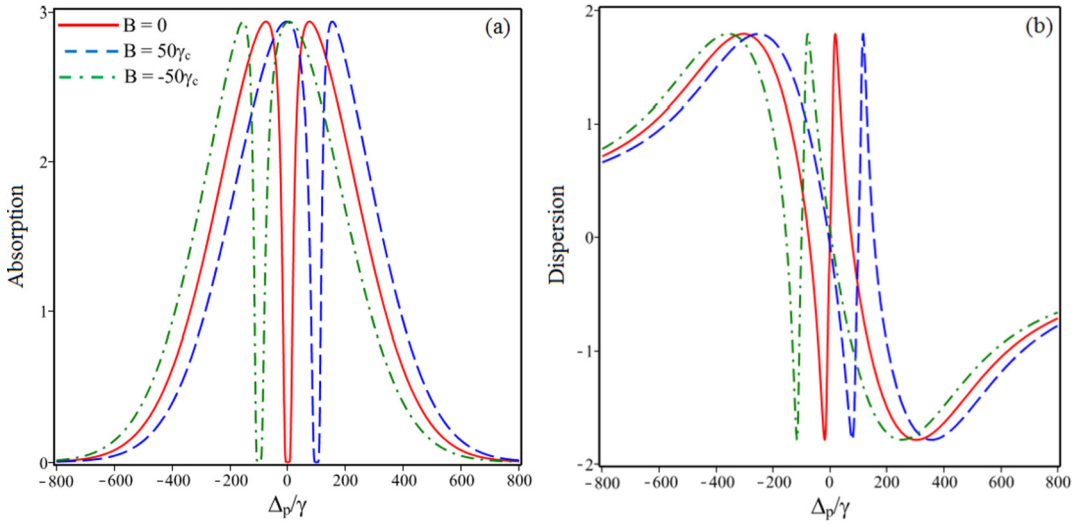

Fig. 2. Absorption (a) and dispersion (b) versus probe field detuning when $\Omega_c = 150\gamma$, $\Delta_c = 0$, T = 300 K, and B = 0 (solid line), B = $50\gamma_c$ (dashed line) and B = $-50\gamma_c$ (dash-dotted line).

$\Delta_c + (v/c)\omega_c$. The numbers of atoms having velocity v which lie along the laser beams obey a Maxwellian distribution:

$$dN(v) = \frac{N_0}{u\sqrt{\pi}} e^{-v^2/u^2} dv, \tag{13}$$

where, $u = \sqrt{2k_B T/m}$, is the root mean square atomic velocity and N_0 is the total atomic density of the atomic medium. Therefore, the susceptibility expressions must be modified to

$$\chi^{(1)}(v)dv = \frac{iN_0 d_{21}^2}{u\sqrt{\pi}\varepsilon_0\hbar}\left(1 - \frac{4\gamma_{31}}{2\gamma + \gamma_{21}}\right)\frac{e^{-v^2/u^2}}{2Z(v)}dv, \tag{14}$$

$$\chi^{(3)}(v)dv = -\frac{iN_0 d_{21}^4}{6u\sqrt{\pi}\varepsilon_0\hbar^3}\left(\frac{1}{2\gamma + \gamma_{21}}\right)\frac{e^{-v^2/u^2}}{Z(v)} \times \left[\frac{1}{Z(v)} + \frac{1}{Z^*(v)}\right]dv, \tag{15}$$

where

$$Z(v) = \gamma - i\left(\Delta_p - \Delta_B + \frac{v}{c}\omega_p\right) + \frac{\Omega_c^2/4}{\gamma_{31} - i(\Delta_p - \Delta_c - 2\Delta_B) - i\frac{v}{c}(\omega_p - \omega_c)}. \tag{16}$$

By integrating Eqs. (14) and (15) over the velocity v from $-\infty$ to $+\infty$, we obtain:

$$\chi^{(1)} = \frac{iN_0 d_{21}^2\sqrt{\pi}}{2\varepsilon_0\hbar\left(\omega_p u/c\right)}\left(1 - \frac{4\gamma_{31}}{2\gamma + \gamma_{21}}\right)e^{z^2}[1 - erf(z)], \tag{17}$$

$$\chi^{(3)} = -\frac{iN_0 d_{21}^4}{6\sqrt{\pi}\varepsilon_0\hbar^3\left(\omega_p u/c\right)^2}\left(\frac{1}{2\gamma + \gamma_{21}}\right) \times \left\{2\sqrt{\pi}\left(-1 + \sqrt{\pi}ze^{z^2}[1 - erf(z)]\right) + \frac{\pi\left(e^{z^2}[1 - erf(z)] + e^{z^{*2}}[1 - erf(z^*)]\right)}{z + z^*}\right\}, \tag{18}$$

where

$$z = \frac{c}{\omega_p u}\left(\gamma - i(\Delta_p - \Delta_B) + \frac{\Omega_c^2/4}{\gamma_{31} - i(\Delta_p - \Delta_c - 2\Delta_B)}\right) = \frac{c}{\omega_p u}Z, \tag{19}$$

z^* is the complex conjugation of z, and erf is the error function.

From the first- and third-order susceptibilities, we determine the linear dispersion n_0 and the self-Kerr nonlinear n_2 coefficients under Doppler effect as [3]:

$$n_0 = \sqrt{1 + \mathrm{Re}(\chi^{(1)})}, \tag{20}$$

$$n_2 = \frac{3\,\mathrm{Re}(\chi^{(3)})}{4\varepsilon_0 n_0^2 c}. \tag{21}$$

3. Results and discussion

In this section, we apply the analytical results to ^{87}Rb atomic vapor. The states $|1\rangle$, $|2\rangle$ and $|3\rangle$ can be chosen as $5S_{1/2}(F = 1, m_F = +1)$, $5P_{1/2}(F = 2, m_F = 0)$, and $5S_{1/2}(F = 2, m_F = -1)$, respectively. The atomic parameters are [33,34]: $N = 4.5 \times 10^{17}$ atoms/m^3, $\gamma_{21} = \gamma_{23} = 2\pi \times 5.3$ MHz, $d_{21} = 1.6 \times 10^{-29}$ C.m. The Landé factor $g_F = -1/2$, and the Bohr magneton $\mu_B = 9.27401 \times 10^{-24}$ JT^{-1}. For simplicity, all quantities related to frequency are given in units γ which should be in the order of MHz for rubidium sodium atoms. In this approach, when the Zeeman shift Δ_B is scaled by γ, then the magnetic field strength B should be in units of the combined constant $\gamma_c = \gamma\hbar/(\mu_B g_F)$ which also has the units of the Tesla. For example, when taking the Zeeman shift $\Delta_B = 50\gamma$, then the magnetic field strength $B = \Delta_B\hbar/(\mu_B m_F g_F) = 50\gamma_c = 37.68 \times 10^{-3}$ T = 376.8 G.

First of all, we demonstrate that it is possible to use the external magnetic field to switch electromagnetically induced transparency (EIT) into electromagnetically induced absorption (EIA) at the resonant frequency region, as depicted in Fig. 2 (a). As shown in the figure, the position of the transparency window has been shifted to the short or long wavelength domain by adjusting the magnitude and the sign of the magnetic field. Specifically, for the case that no magnetic field is applied (i.e., B = 0 which corresponds to $\Delta_B = 0$), the position of the transparency window is localized at line center of the absorption profile. However, when the external magnetic field is switched on, the transparency window has moved to the left by an amount of $\Delta_p = 100\gamma$ for the case of B = $-50\gamma_c$ (which corresponds to $\Delta_B = -50\gamma$) and moved to the right by the same amount $\Delta_p = 100\gamma$ for the case of B = $-50\gamma_c$ (which corresponds to $\Delta_B = 50\gamma$). These lead to the appearance of an absorption peak at the line center, that is, it has been switched from transparent to absorbed regimes. This phenomenon can be used for optical switching in photonic devices

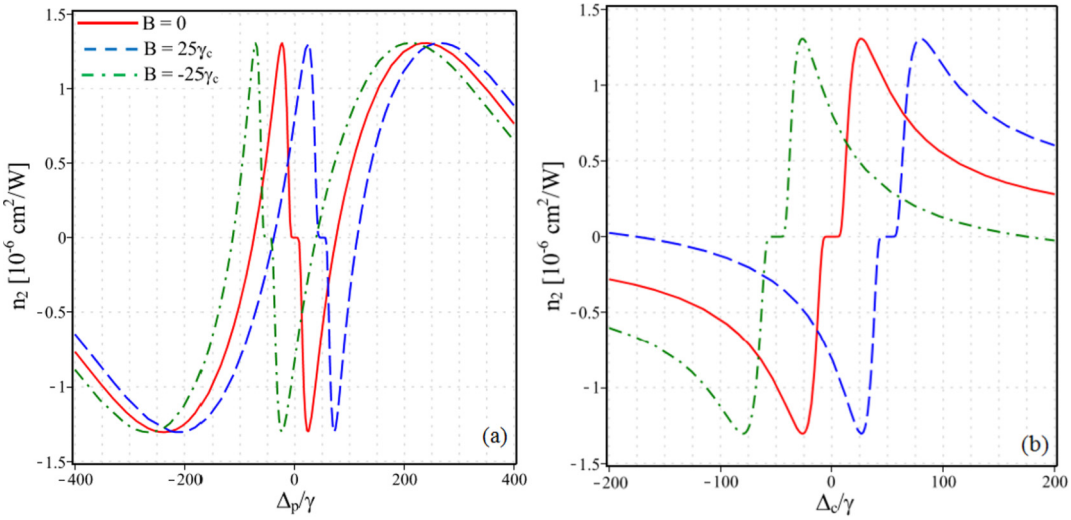

Fig. 3. Variations of the Kerr nonlinear coefficient versus probe field detuning when $\Delta_c = 0$ (a) and versus coupling field detuning when $\Delta_p = 0$ (b). Other parameters are $\Omega_c = 150\gamma$, T = 300 K, and B = 0 (solid line), B = $25\gamma_c$ (dashed line) and B = $-25\gamma_c$ (dash-dotted line).

[33]. Along with the transition between EIT and EIA, the dispersion is also switched from normal to abnormal regimes in the resonant domain via turn-on/off of the external magnetic field, as shown in Fig. 2(b). Therefore, we can use the external magnetic field as a "knob" to switch the light propagation modes from superluminal to subluminal and vice versa.

Next, we demonstrate that it is possible to use the external magnetic field to switch a negative peak of the Kerr nonlinear coefficient into a positive peak and vice versa, as shown in Fig. 3. In Fig. 3(a), we fix the coupling field detuning at $\Delta_c = 0$ and plot the Kerr nonlinear coefficient versus probe field detuning Δ_p for different values of the external magnetic field B = 0 (solid line), B = $25\gamma_c$ (dashed line) and B = $-25\gamma_c$ (dash-dotted line). It shows that the negative peak of the Kerr nonlinear coefficient at $\Delta_p = 25\gamma$ in the case of B = 0 has switched to the positive peak when B = $25\gamma_c$. Similarly, the positive peak of the Kerr nonlinear coefficient at $\Delta_p = -25\gamma$ in the case of B = 0 has switched to the negative peak when B = $-25\gamma_c$. Moreover, similar to linear dispersion, here, nonlinear dispersion is also transformed from normal to anomalous when turn-on/off of the external magnetic field. In Fig. 3(b), we fix the probe field frequency at $\Delta_p = 0$ and plot the Kerr nonlinear coefficient versus coupling field detuning Δ_c for different values of the external magnetic field B = 0 (solid line), B = $25\gamma_c$ (dashed line) and B = $-25\gamma_c$ (dash-dotted line). It is clearly shown that the positive peak of the Kerr nonlinear coefficient at $\Delta_c = 25\gamma$ and the negative peak at $\Delta_c = -25\gamma$ in the case of B = 0 have switched to the negative peak when B = $25\gamma_c$ and the positive peak when B = $-25\gamma_c$, respectively. Moreover, this figure also shows that the Kerr nonlinear coefficient is controlled not only by the external magnetic field, but also by the coupling field detuning.

In particular, the zero value of the Kerr nonlinear coefficient at two-photon resonance of probe and coupling lights ($\Delta_p = \Delta_c = 0$) in the case of B = 0 (see the solid line of Fig. 3a) can be transformed to the positive peak when B = $12\gamma_c$ and the negative peak when B = $-12\gamma_c$, as depicted in Fig. 4. This means that we can use the external magnetic field to move a peak of enhanced Kerr nonlinearity into resonant domain with reduced absorption. Thus, by increasing or decreasing the external magnetic field strength, the Kerr nonlinear coefficient can be changed not only in magnitude but also in its sign.

In Fig. 5 we examine the variation of the Kerr nonlinear coefficient with respect to the coupling field intensity when fixed other parameters at $\Delta_p = 25\gamma$, $\Delta_c = 0$, and T = 300 K (which cor-

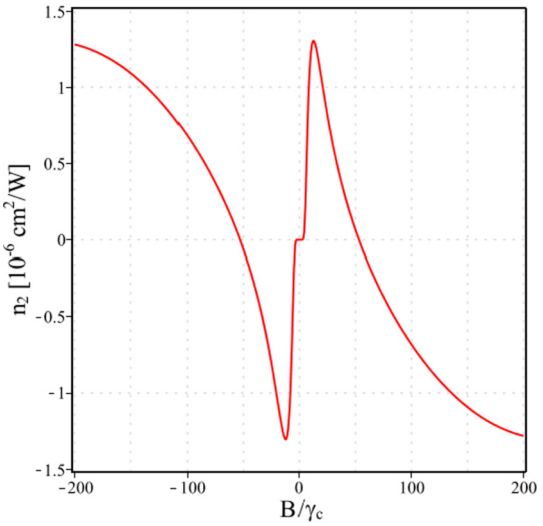

Fig. 4. Change of the magnitude and the sign of the Kerr nonlinear coefficient versus the external magnetic field when $\Delta_p = 0$, $\Delta_c = 0$, $\Omega_c = 150\gamma$ and T = 300 K.

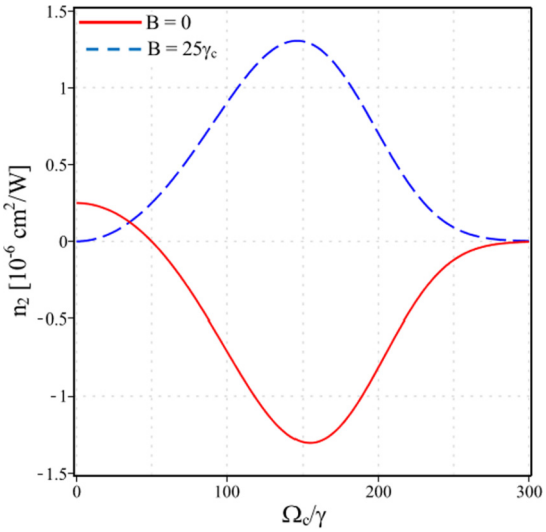

Fig. 5. Variation of the Kerr nonlinear coefficient versus the coupling field intensity when $\Delta_p = 25\gamma$, $\Delta_c = 0$ and T = 300 K.

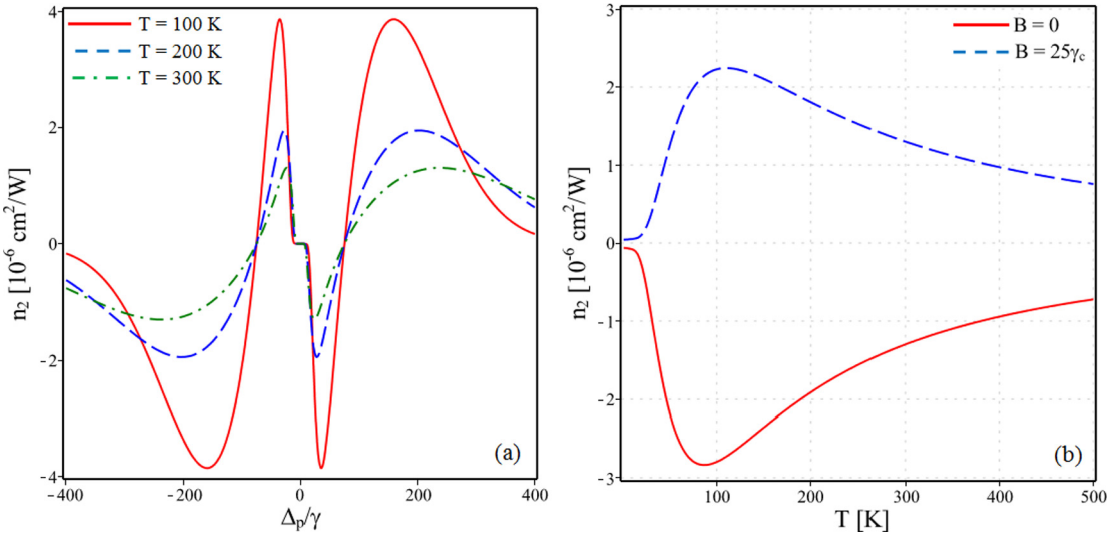

Fig. 6. (a) Variation of the Kerr nonlinear coefficient versus probe field detuning when $B = 0$, $\Delta_c = 0$, $\Omega_c = 150\gamma$, and $T = 100$ K (solid line), $T = 200$ K (dashed line) and $T = 300$ K (dash-dotted line). (b) Variation of the Kerr nonlinear coefficient versus absolute temperature when $\Delta_p = 25\gamma$, $\Delta_c = 0$, $\Omega_c = 150\gamma$, and $B = 0$ (dashed line) and $B = 25\gamma_c$ (solid line).

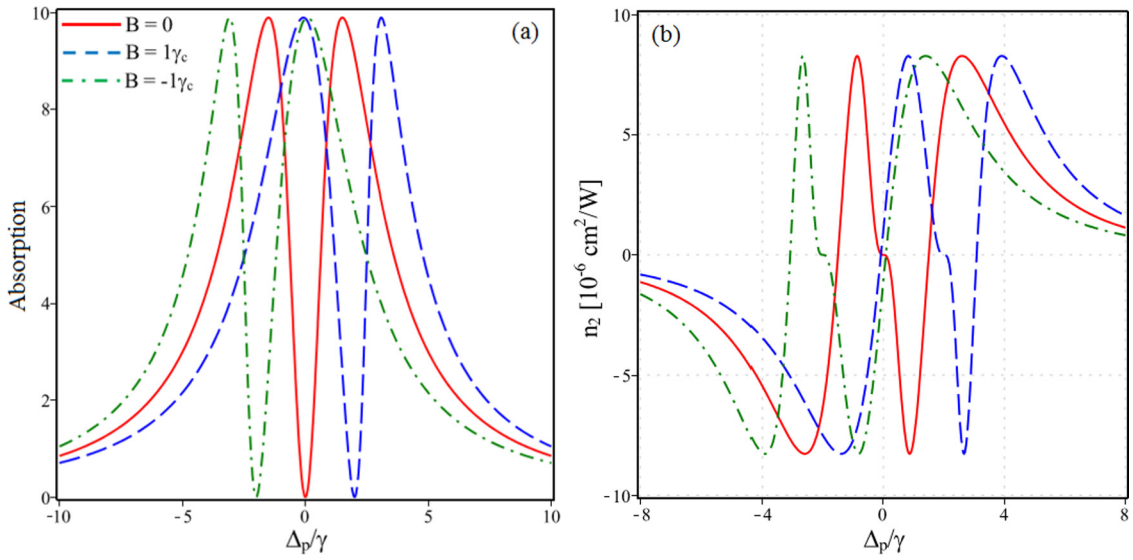

Fig. 7. Variations of absorption (a) and Kerr nonlinear coefficients (b) versus probe field detuning in the case of Doppler free when $\Omega_c = 3\gamma$, $\Delta_c = 0$, and $B = 0$ (solid line), $B = 1\gamma_c$ (dashed line) and $B = -1\gamma_c$ (dash-dotted line).

responds to the maximum point in the solid line of Fig. 3a), for the cases when $B = 0$ (solid line) and $B = 25\gamma_c$ (dashed line). It sees that the amplitude and slope of Kerr nonlinear curve can be changed by tuning of the coupling field intensity. In particular, by choosing the magnetic field strength $B = 25\gamma_c$, the variation of the Kerr nonlinear coefficient versus the coupling field intensity is opposite to that when $B = 0$.

Finally, we investigate the influence of Doppler broadening on the magnitude of the Kerr nonlinear coefficient as presented in Fig. 6. In Fig. 6(a), we plot the Kerr nonlinear coefficient with respect to the probe field detuning for different values of the temperature in the case of $B = 0$. It is clear that an increase in temperature leads to the decrease in amplitude of the Kerr nonlinearity and the extension in the nonlinear dispersion profile. In Fig. 6(b) we plot the Kerr nonlinear coefficient versus the absolute temperature at the fixed parameters are $\Delta_p = 25\gamma$, $\Delta_c = 0$, $\Omega_c = 150\gamma$, and $B = 0$ (dashed line) and $B = 25\gamma_c$ (solid line) which corresponding to the maximum point of nonlinear coefficient in Fig. 6a. From Fig. 6(b) we find that, for the given values of parameters Δ_c, Δ_p, and Ω_c we can choose an optimized temperature to obtain the largest value of the Kerr nonlinear coefficient. In addition, we can choose the magnetic field strength $B = 25\gamma_c$ so that the variation of the Kerr nonlinear coefficient versus the coupling field intensity is opposite to that when $B = 0$. On the other hand, from the above considerations, it can be seen that under Doppler broadening (at room temperature, for example) the Zeeman shift of the levels $|1\rangle$ and $|3\rangle$ needs to be large enough to overcome the overlap between levels $|1\rangle$ and $|3\rangle$, so a strong magnetic field is required. However, in the case of Doppler free (for cold atoms), such results can be obtained with a much smaller magnetic field, as shown in Fig. 7.

4. Conclusion

We have derived the analytical expression for the self-Kerr nonlinear coefficient in a degenerate two-level atomic medium under Doppler broadening. The magnitude and the sign of the self-Kerr nonlinear coefficient are simply controlled by the external mag-

netic field as well as the frequency and intensity of coupling field. By choosing the appropriate external magnetic field we can switch a negative peak of the Kerr nonlinear coefficient into a positive peak and vice versa, and transform a zero value of the Kerr nonlinear coefficient into a maximum value at resonant frequency. In addition, under Doppler broadening the external magnetic field (and hence Zeeman shift) must be large enough to overcome the overlap between ground-state sublevels. Such a controllable Kerr nonlinear coefficient can be used to control the working characteristics of photonic devices. Moreover, the analytical model is not only convenient for considering the influence of controllable parameters on the Kerr nonlinear coefficient, but it is also easily used to fit the experimental observations under different temperatures.

Declaration of competing interest

The authors declare that they have no known competing financial interests or personal relationships that could have appeared to influence the work reported in this paper.

References

[1] K.J. Boller, A. Imamoglu, S.E. Harris, Observation of electromagnetically induced transparency, Phys. Rev. Lett. 66 (1991) 2593.

[2] H. Schmidt, A. Imamogdlu, Giant Kerr nonlinearities obtained by electromagnetically induced transparency, Opt. Lett. 21 (1996) 1936.

[3] S.E. Harris, L.V. Hau, Nonlinear optics at low light levels, Phys. Rev. Lett. 82 (1999) 4611.

[4] H. Wang, D. Goorskey, M. Xiao, Enhanced Kerr nonlinearity via atomic coherence in a three-level atomic system, Phys. Rev. Lett. 87 (2001) 073601.

[5] Y.P. Niu, S.Q. Gong, Enhancing Kerr nonlinearity via spontaneously generated coherence, Phys. Rev. A 73 (2006) 053811.

[6] X.-a. Yan, L.-q. Wang, B.-y. Yin, W.-j. Jiang, H.-b. Zheng, J.-p. Song, Y.-p. Zhang, Effect of spontaneously generated coherence on Kerr nonlinearity in a four-level atomic system, Phys. Lett. A 372 (2008) 6456–6460.

[7] H.R. Hamedi, G. Juzeliunas, Phase-sensitive Kerr nonlinearity for closed-loop quantum systems, Phys. Rev. A 91 (2015) 053823.

[8] H. Gao, H. Sun, S. Fan, H. Zhang, Phase control of Kerr nonlinearity in V-type system with spontaneously generated coherence, J. Mod. Opt. 63 (2016) 598–604.

[9] S.H. Asadpour, M. Sahrai, A. Soltani, H.R. Hamed, Enhanced Kerr nonlinearity via quantum interference from spontaneous emission, Phys. Lett. A 376 (2012) 147–152.

[10] H. Sun, Y. Niu, S. Jin, S. Gong, Phase control of the Kerr nonlinearity in electromagnetically induced transparency media, J. Phys. B, At. Mol. Opt. Phys. 41 (2008) 065504.

[11] Y.-W. Jiang, K.-D. Zhu, Controlling Kerr nonlinearity with electric fields in asymmetric double quantum-dots, arXiv:0801.3726v1 [cond-mat.mes-hall], 2008.

[12] X.-a. Yan, L.-q. Wang, B.-y. Yin, J.-p. Song, Electromagnetically induced transparency and enhanced self-Kerr nonlinearity in a four-level scheme, Optik 122 (2011) 986–990.

[13] Hessa M.M. Alotaibi, Barry C. Sanders, Enhanced nonlinear susceptibility via double-double electromagnetically induced transparency, Phys. Rev. A 94 (2016) 053832.

[14] J. Sheng, X. Yang, H. Wu, M. Xiao, Modified self-Kerr-nonlinearity in a four-level N-type atomic system, Phys. Rev. A 84 (2011) 053820.

[15] D.X. Khoa, L.V. Doai, D.H. Son, N.H. Bang, Enhancement of self-Kerr nonlinearity via electromagnetically induced transparency in a five-level cascade system: an analytical approach, J. Opt. Soc. Am. B 31 (2014) 1330.

[16] N.H. Bang, D.X. Khoa, D.H. Son, L.V. Doai, Effect of Doppler broadening on giant self-Kerr nonlinearity in a five-level ladder-type system, J. Opt. Soc. Am. B 36 (2019) 3151.

[17] L.V. Doai, N.L.T. An, D.X. Khoa, V.N. Sau, N.H. Bang, Manipulating giant cross-Kerr nonlinearity at multiple frequencies in an atomic gaseous medium, J. Opt. Soc. Am. B 36 (2019) 2856.

[18] L.V. Doai, Giant cross-Kerr nonlinearity in a six-level inhomogeneously broadened atomic medium, J. Phys. B, At. Mol. Opt. Phys. 52 (2019) 225501.

[19] P. Kaur, A. Wasan, Effect of magnetic field on the optical properties of an inhomogeneously broadened multilevel Λ-system in Rb vapor, Eur. Phys. J. D 71 (2017) 78.

[20] B. Vaseghi, N. Mohebi, Effects of external fields, dimension and pressure on the electromagnetically induced transparency of quantum dots, J. Lumin. 134 (2013) 352–357.

[21] N. Ba, X.-Y. Wu, X.-J. Liu, S.-Q. Zhang, J. Wang, Electromagnetically induced grating in an atomic system with a static magnetic field, Opt. Commun. 285 (2012) 3792–3797.

[22] V. Pavlovic, L. Stevanovic, Electromagnetically induced transparency in a spherical quantum dot with hydrogenic impurity in the external magnetic field, Superlattices Microstruct. 92 (2016) 10–23.

[23] H. Cheng, H.-M. Wang, S.-S. Zhang, P.-P. Xin, J. Luo, H.-P. Liu, Electromagnetically induced transparency of ^{87}Rb in a buffer gas cell with magnetic field, J. Phys. B, At. Mol. Opt. Phys. 50 (2017) 095401.

[24] K. Cox, V.I. Yudin, A.V. Taichenachev, I. Novikova, E.E. Mikhailov, Measurements of the magnetic field vector using multiple electromagnetically induced transparency resonances in Rb vapor, Phys. Rev. A 83 (2011) 015801.

[25] D. Slavov, A. Sargsyan, D. Sarkisyan, R. Mirzoyan, A. Krasteva, A.D. Wilson-Gordon, S. Cartaleva, Sub-natural width N-type resonance in cesium atomic vapour: splitting in magnetic fields, J. Phys. B, At. Mol. Opt. Phys. 47 (2014) 035001.

[26] S. Mitra, S. Dey, M.M. Hossain, P.N. Ghosh, B. Ray, Temperature and magnetic field effects on the coherent and saturating resonances in Λ- and V-type systems for the ^{85}Rb-D_2 transition, J. Phys. B, At. Mol. Opt. Phys. 46 (2013) 075002.

[27] C. Mishra, A. Chakraborty, A. Srivastava, S.K. Tiwari, S.P. Ram, V.B. Tiwari, S.R. Mishr, Electromagnetically induced transparency in Λ-systems of ^{87}Rb atom in magnetic field, J. Mod. Opt. 65 (2018) 2269–2277.

[28] S.H. Asadpour, H.R. Hamedi, H.R. Soleimani, Slow light propagation and bistable switching in a graphene under an external magnetic field, Laser Phys. Lett. 12 (2015) 045202.

[29] R. Karimi, S.H. Asadpour, S. Batebi, H.R. Soleimani, Manipulation of pulse propagation in a four-level quantum system via an elliptically polarized light in the presence of external magnetic field, Mod. Phys. Lett. B 29 (2015) 1550185.

[30] R. Yu, J. Li, C. Ding, X. Yang, Dual-channel all-optical switching with tunable frequency in a five-level double-ladder atomic system, Opt. Commun. 284 (2011) 2930–2936.

[31] J. Li, R. Yu, L. Si, X. Yang, Propagation of twin light pulses under magneto-optical switching operations in a four-level inverted-Y atomic medium, J. Phys. B, At. Mol. Opt. Phys. 43 (2010) 065502.

[32] D. Zhang, R. Yu, C. Ding, H. Huang, Z. Sun, X. Yang, Phase control of optical bistability and multistability in closed-type Landau-quantized grapheme, Laser Phys. Lett. 13 (2016) 125201.

[33] H.M. Dong, L.T.Y. Nga, N.H. Bang, Optical switching and bistability in a degenerated two-level atomic medium under an external magnetic field, Appl. Opt. 58 (2019) 4192.

[34] Daniel Adam Steck, Rb^{87} D Line Data, http://steck.us/alkalidata.